the LRM are also seen in the MASCS data (*30*). From these observations and previous work (*2*–*7*, *10*, *18*, *21*), we propose that Mercury's crust is composed of iron-poor calcium-magnesium silicates (e.g., plagioclase, enstatite, pigeonite, and diopside) with a detectable component of spectrally neutral opaque minerals. Ilmenite ($FeTiO_3$) is the most likely candidate based on lunar analogy and cosmochemical abundance considerations. This lithology is broadly basaltic to gabbroic, with nearly all ferrous iron contained in opaque minerals and not in silicates, requiring redox conditions at or near the iron-wüstite buffer. An alternative to ilmenite is native iron metal, but such a material is relatively red at typical lunar regolith grain sizes (*29*, *31*) and implies more reducing conditions than iron-wüstite. The distinctively red smooth plains (HRP) appear to be large-scale volcanic deposits stratigraphically equivalent to the lunar maria (*20*), and their spectral properties (steeper spectral slope) are consistent with magma depleted in opaque materials. The large areal extent (>10^6 km^2) of the Caloris HRP is inconsistent with the hypothesis that volcanism was probably shallow and local (*10*); rather, such volcanism was likely a product of extensive partial melting of the upper mantle.

References and Notes

1. S. E. Hawkins III *et al.*, *Space Sci. Rev.* **131**, 247 (2007).
2. T. B. McCord, J. B. Adams, *Icarus* **17**, 585 (1972).
3. B. Hapke, G. E. Danielson Jr., K. Klaasen, L. Wilson, *J. Geophys. Res.* **80**, 2431 (1975).
4. J. Warell, *Icarus* **161**, 199 (2003).
5. F. Vilas, in *Mercury*, F. Vilas, C. R. Chapman, M. S. Mathews, Eds. (Univ. of Arizona Press, Tucson, 1988), pp. 59–76.
6. A. L. Sprague, T. L. Roush, *Icarus* **133**, 174 (1998).
7. J. Warell, D. T. Blewett, *Icarus* **168**, 257 (2004).
8. B. Hapke, *J. Geophys. Res.* **106**, 10039 (2001).
9. B. Hapke, C. Christman, B. Rava, J. Mosher, *Proc. Lunar Planet Sci. Conf.* **11**, 817 (1980).
10. B. Rava, B. Hapke, *Icarus* **71**, 397 (1987).
11. M. S. Robinson, P. G. Lucey, *Science* **275**, 197 (1997).
12. M. S. Robinson, G. J. Taylor, *Meteorit. Planet. Sci.* **36**, 841 (2001).
13. M. Minnaert, in *Planets and Satellites*, G. P. Kuiper, B. M. Middlehurst, Eds. (Univ. of Chicago Press, Chicago, 1961), pp. 213–248.
14. J. Veverka, P. Helfenstein, B. Hapke, J. D. Goguen, in *Mercury*, F. Vilas, C. R. Chapman, M. S. Matthews, Eds. (Univ. of Arizona Press, Tucson, 1988), pp. 37–58.
15. P. D. Spudis, J. E. Guest, in *Mercury*, F. Vilas, C. R. Chapman, M. S. Mathews, Eds. (Univ. Arizona Press, Tucson, 1988), pp. 118–164.
16. R. G. Strom *et al.*, *Science* **321**, 79 (2008).
17. D. Dzurisin, *Geophys. Res. Lett.* **4**, 383 (1977).
18. B. W. Denevi, M. S. Robinson, *Icarus*, in press 10.1016/j.icarus.2008.04.021 (2008).
19. J. W. Head *et al.*, *Science* **321**, 69 (2008).
20. S. L. Murchie *et al.*, *Science* **321**, 73 (2008).
21. J. Warell, *Icarus* **167**, 271 (2004).
22. P. G. Lucey, D. T. Blewett, B. L. Jolliff, *J. Geophys. Res.* **105**, 20297 (2000).
23. G. Heiken, D. T. Vaniman, B. M. French, *Lunar Sourcebook: A User's Guide to the Moon* (Cambridge Univ. Press, New York, 1991).
24. S. K. Noble, C. M. Pieters, *Sol. Syst. Res.* **37**, 31 (2003).
25. M. J. Cintala, *J. Geophys. Res.* **97**, 947 (1992).
26. D. T. Blewett, B. R. Hawke, P. G. Lucey, *Meteorit. Planet. Sci.* **37**, 1245 (2002).
27. B. R. Hawke, P. G. Lucey, J. F. Bell, R. Jaumann, G. Neukum, *Lunar Planet. Sci.* **17**, 999 (1986).
28. M. A. Riner, M. S. Robinson, J. A. Tangeman, R. C. Elphic, *Lunar Planet. Sci.* **36**, abstract 1943 (2005).
29. E. A. Cloutis et al., *Icarus*, in press; doi:10.1016/j.icarus.2008.04.018 (2008).
30. W. E. McClintock *et al.*, *Science* **321**, 62 (2008).
31. E. A. Cloutis, D. T. Bailey, M. A. Craig, P. S. Harderson, *Lunar Planet. Sci.* **39**, abstract 1082 (2008).

32. The hundreds of engineers and technical support personnel who brought MESSENGER from a concept to a successful flight project warrant the sustained appreciation of the mission science team. N. Laslo, H. Kang, R. Vaughan, A. Harch, R. Shelton, and A. Berman designed the imaging sequences that made this contribution possible. B. Denevi, K. Becker, and C. Hash are gratefully acknowledged for data calibration and processing. The MESSENGER project is supported by the NASA Discovery Program under contracts NAS5-97271 to Johns Hopkins University Applied Physics Laboratory and NASW-00002 to the Carnegie Institution of Washington.

6 May 2008; accepted 3 June 2008
10.1126/science.1160080

REPORT

Volcanism on Mercury: Evidence from the First MESSENGER Flyby

James W. Head,[1]* Scott L. Murchie,[2] Louise M. Prockter,[2] Mark S. Robinson,[3] Sean C. Solomon,[4] Robert G. Strom,[5] Clark R. Chapman,[6] Thomas R. Watters,[7] William E. McClintock,[8] David T. Blewett,[2] Jeffrey J. Gillis-Davis[9]

The origin of plains on Mercury, whether by volcanic flooding or impact ejecta ponding, has been controversial since the Mariner 10 flybys (1974–75). High-resolution images (down to 150 meters per pixel) obtained during the first MESSENGER flyby show evidence for volcanic vents around the Caloris basin inner margin and demonstrate that plains were emplaced sequentially inside and adjacent to numerous large impact craters, to thicknesses in excess of several kilometers. Radial graben and a floor-fractured crater may indicate intrusive activity. These observations, coupled with additional evidence from color images and impact crater size-frequency distributions, support a volcanic origin for several regions of plains and substantiate the important role of volcanism in the geological history of Mercury.

Volcanic deposits provide important clues to mantle composition, the location of past interior thermal anomalies, and the general thermal evolution of a planet. Relative to the other terrestrial planets, little is known with certainty concerning the history of volcanism on Mercury. In the more than three decades since Mariner 10 flew by Mercury in 1974–75, debate has persisted about the presence or absence of volcanic deposits (*1*), a question we address with data from the first flyby of Mercury by MESSENGER.

Whereas the Moon has distinctive composition-related differences in reflectance between highlands and volcanic maria, the reflectance of Mercury and of its smooth plains is relatively uniform, and therefore the role of volcanism is less obvious. Mariner 10 images, obtained shortly after the Apollo 16 mission to the Moon, revealed two widespread plains units that are similar to the lunar Cayley light plains (*2*, *3*): smooth plains and intercrater plains (*4*). These plains deposits on Mercury were interpreted to be volcanic in origin, on the basis of their smoothness and apparent ponding and embayment of lowland terrain (*4*, *5*). Other researchers, influenced by Apollo 16 results showing that similar-appearing deposits on the Moon were impact breccias, argued that Mercury's smooth plains represented basin ejecta deposits (*3*, *6*). The relatively low resolution of Mariner 10 images (typically ~1 km per pixel) was insufficient to resolve this issue. Lunar-like volcanic features, such as small shields, cones, sinuous rilles, and other vent-related structures, were not detected in Mariner 10 images (*7*, *8*), and the features that were observed did not provide conclusive evidence of a volcanic origin. For example, lobate fronts exposed at the edge of smooth plains suggested the presence of volcanic flow margins on Mercury, but similar features have been identified on the margins of lunar basin ejecta flows (*8*, *9*). The density of impact craters on Caloris

[1]Department of Geological Sciences, Brown University, Providence, RI 02912, USA. [2]Johns Hopkins University Applied Physics Laboratory, Laurel, MD 20723, USA. [3]School of Earth and Space Exploration, Arizona State University, Tempe, AZ 85287, USA. [4]Department of Terrestrial Magnetism, Carnegie Institution of Washington, Washington, DC 20015, USA. [5]Lunar and Planetary Laboratory, University of Arizona, Tucson, AZ 85721, USA. [6]Southwest Research Institute, 1050 Walnut Street, Boulder, CO 80302, USA. [7]Center for Earth and Planetary Studies, National Air and Space Museum, Smithsonian Institution, Washington, DC 20560, USA. [8]Laboratory for Atmospheric and Space Physics, University of Colorado, Boulder, CO 80303, USA. [9]Hawaii Institute of Geophysics and Planetology, University of Hawaii, Honolulu, HI 96822, USA.

*To whom correspondence should be addressed. E-mail: James_Head@brown.edu

basin ejecta and nearby smooth plains deposits suggested that the plains were emplaced after the Caloris basin had formed (*10*), providing evidence that they might be volcanic in origin, not contemporaneous ejecta emplacement. Some lunar Cayley plains, however, display younger ages than adjacent basin ejecta (*11*). Reprocessed Mariner 10 color data (*12*) show color boundaries for smooth plains units, suggesting a distinctive mineralogy. Theoretical studies (*8*, *9*) indicate that a thick low-density crust could inhibit effusive eruptions, particularly if aided by global compression (*13*). Thus, conclusive evidence was lacking for the origin of smooth and intercrater plains and for establishing the role of volcanism in the history of Mercury (*1*, *14*).

The first MESSENGER flyby of Mercury has provided high-resolution multispectral images of regions both seen and unseen by Mariner 10, including the interior plains of the Caloris basin, the circum-Caloris region characterized by smooth plains, and regions of smooth and intercrater plains near the terminator. The data show a variety of evidence for volcanic features and deposits across this part of the planet. The new images (Figs. 1 to 4) reveal several volcanic vents and related deposits distributed along the southern margins of the Caloris basin interior and characterized by distinctive color anomalies (*15*, *16*) (Fig. 1). Several irregularly shaped rimless depressions are surrounded by smoother deposits that have albedos differing from those of surrounding units. For example, along the southern margin of Caloris, a kidney-shaped depression about 20 km long is centered on a smooth deposit that is greater than 100 km in diameter (Fig. 1). A relatively bright deposit that surrounds the kidney-shaped depression to a radial distance of about 25 km appears to discolor or mantle the underlying terrain and becomes more diffuse toward its edges. Several small irregular depressions are observed in the southwestern part of the smooth deposit. Each has an irregular shape similar to those of volcanic vents on other planetary bodies, unlike the generally circular shapes of primary craters and elongated secondary craters with rims. These features and their close association with the distinctive smooth deposits imply that these broad structures are volcanic vents.

Although altimetry data are not available for this region, several lines of evidence suggest that the broad feature is domelike in nature (Fig. 1). The decrease in brightness along the northwestern deposit is consistent with a surface sloping away from the kidney-shaped depression in the downsun direction. Small massifs at the Caloris basin rim to the southwest appear to be partially buried, which suggests that they are covered by volcanic deposits from this region. Finally, two large impact craters (~25 to 30 km across) straddle the northwestern edge of the deposit. Both contain interior deposits (walls and rough floors) that are typical of impact craters of this size (*17*) and seen elsewhere in Fig. 1. The rim and exterior deposits differ between the two craters, however: The eastern rim of the southernmost crater is heavily embayed (toward the central part of the feature) such that its rim crest is no longer visible. Rim heights of fresh Mercury craters of the same size (*17*) imply that about 800 m of lava would be required to flood the crater to the level of the rim crest. Thus, on the basis of these lines of evidence, we interpret this structure to be a broad, low shield volcano similar in character to mare domes on the Moon that erupted a sequence of lava flows (*18*). At least four similar examples are seen in the southern part of the interior Caloris basin rim (*15*). The diffuse-bordered bright halo surrounding the kidney-shaped depression in Fig. 1 is interpreted to consist of pyroclastic deposits emplaced from vent-centered eruptions, on the grounds that similar kidney-shaped depressions and pyroclastic deposits have been documented on the Moon (*19*).

MESSENGER images show that many impact craters and areas between craters have been flooded with lava. Large fresh impact craters (Fig. 2A) have rough flat floors; central peaks and peak rings; terraced walls; and—beyond the interior—a sharp rim crest, raised rim, and radially textured ejecta. Crater chains and crater clusters are seen in many exterior ejecta deposits. Volcanically modified impact craters on the Moon, such as Archimedes crater within the Imbrium basin (*20*), have a shallow, smooth crater floor, a lack of peaks and peak rings, and flooded and embayed exterior deposits.

The morphology of a large, degraded ~240-km-diameter impact crater near the terminator offers an opportunity to compare fresh and degraded craters and the processes responsible for their modification (Fig. 2B). The crater is located far from the Caloris basin rim (1375 km to the southwest), and there is no radial texture suggestive of ejecta emplacement from a nearby impact basin. Smooth plains nearly fill the crater and also embay the interior crater walls, which is suggestive of volcanic flooding. Five smaller impact craters are superposed on the degraded crater: Three lie on the rim crest, one lies outside the crater (to the northwest), and one lies on the southern part of the crater floor. In contrast to fresh craters (Fig. 2A), the 85-km-diameter crater on the southern crater floor has been embayed along its northern margin up to the base of the raised rim, and all of its exterior ejecta have been buried by the emplacement of plains, which also flood its interior. Similar relations are seen on the three craters on the degraded crater rim. Crater floor plains embay the exterior ejecta of each of these craters, up to the base of their respective raised rims, although exterior ejecta deposits are preserved elsewhere on the degraded crater rim. Ejecta from the large superposed crater to the northwest, once present on the floor of the degraded crater, are now buried by smooth plains. Small "ghost" craters, apparently buried by plains emplacement, are also observed (Fig. 2C).

Fresh craters with diameters similar to that of the large degraded crater are generally more than 5 km deep (*17*), and yet this crater has undergone substantial shallowing. The degraded state of the crater and the superposition of numerous large craters on it imply an extended interval of modification. Moreover, the embayment and burial of the exterior deposits of each of these craters by smooth plains suggest that more recent and sequential volcanic flooding was involved. In addition, the presence of flowlike scarps and ghost craters, the lack of basin ejecta sculpture, and the distance from known basins all combine to favor a volcanic origin for the emplacement of these

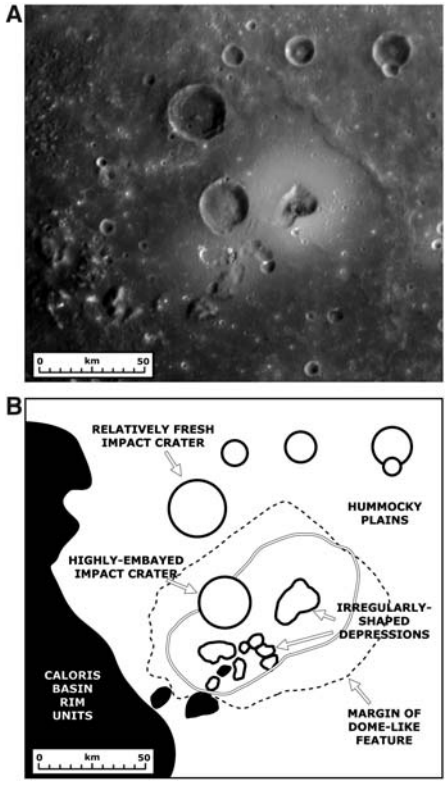

Fig. 1. Central kidney-shaped depression superposed on a broad, smooth domelike feature and surrounded by bright halo material. As one of several similar features along the inner margin of the southern Caloris basin rim [bottom left in (A) and (B)], this feature resembles small shield volcanoes on the Moon (*18*) and is interpreted as a volcanic vent. (**A**) Dome and kidney-shaped depression [mosaic of Mercury Dual Imaging System narrow-angle camera (MDIS NAC) images EN0108826812M and EN0108826877M, centered at 22.5°N, 146.2°E]. North is to the top in this and subsequent images. (**B**) Sketch map illustrating the main features and relationships. The paired lines enclose bright material surrounding depressions. This and the following images are at 750-nm wavelength. Locations on Mercury of this and the following images are shown in the supporting online material of (*29*).

crater interior plains. Subsequent to flooding, a large northeast-to-southwest–trending fault scarp (Fig. 2, B and C) cut the interior superposed crater and the southern part of the degraded crater.

On the Moon and Mars, volcanically flooded impact craters are often outlined by circular wrinkle-ridge patterns (*21*) (Fig. 3B). The rim crests of impact craters that are almost completely flooded by lavas act to localize deformation of the volcanic sequence, forming the wrinkle-ridge ring. MESSENGER near-terminator image data reveal a large (~60-km-diameter) wrinkle-ridge ring in an area of extensive smooth plains (Fig. 3A). Several small knobs, interpreted to be the remnants of the crater rim crest, are all that remain of the crater. This structure interrupts a regional northeast-trending pattern of wrinkle ridges. If the current ring diameter (60 km) is a good approximation of the original size of the crater, about 2.7 km of lava fill would be required to flood the original crater to its rim crest (*17*). Several other wrinkle-ridge rings are observed in this region. These observations further attest to the emplacement of substantial thicknesses of volcanic plains.

Intrusive activity is a prerequisite for volcanism, and the MESSENGER data reveal possible candidates for shallow sills and dikes. On the Moon, fractures on crater floors have been interpreted to form either by viscous relaxation (*22*) or the intrusion of sills and uplift of crater floors (*23*). The presence of floor-fractured craters was suspected from Mariner 10 data (*24*), and the MESSENGER data confirm their presence (Fig. 4). A ~35-km-diameter crater, located near the margins of the extensive plains units, shows two fractured domes on its floor (Fig. 4). The local-

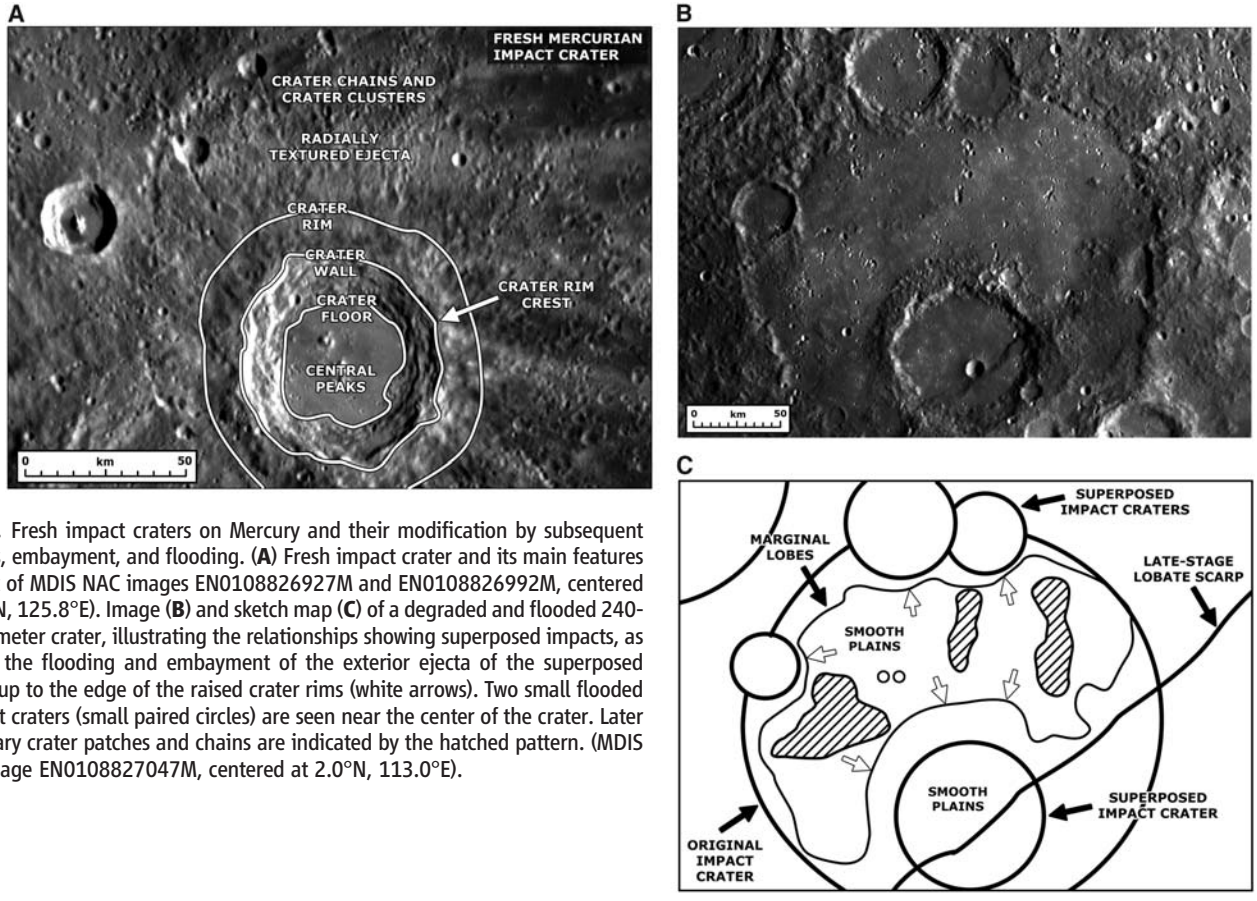

Fig. 2. Fresh impact craters on Mercury and their modification by subsequent impacts, embayment, and flooding. (**A**) Fresh impact crater and its main features (mosaic of MDIS NAC images EN0108826927M and EN0108826992M, centered at 9.6°N, 125.8°E). Image (**B**) and sketch map (**C**) of a degraded and flooded 240-km-diameter crater, illustrating the relationships showing superposed impacts, as well as the flooding and embayment of the exterior ejecta of the superposed craters up to the edge of the raised crater rims (white arrows). Two small flooded or ghost craters (small paired circles) are seen near the center of the crater. Later secondary crater patches and chains are indicated by the hatched pattern. (MDIS NAC image EN0108827047M, centered at 2.0°N, 113.0°E).

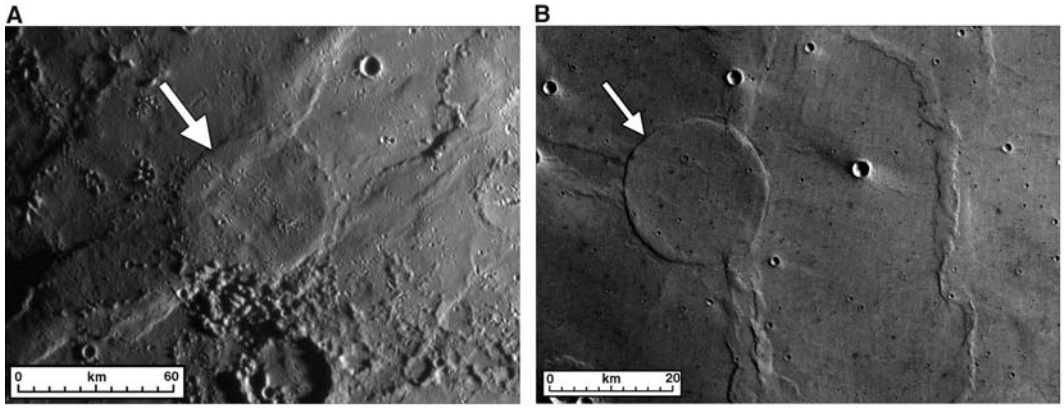

Fig. 3. Wrinkle-ridge rings on Mercury and Mars. These features are interpreted to be impact craters almost completely flooded by lavas; subsequent regional deformation forms linear wrinkle ridges whose regional patterns are disrupted into rings by the presence of the buried crater rim. (**A**) Near-terminator view of a ~60-km-diameter wrinkle-ridge ring in an area of extensive smooth plains (MDIS NAC image EN0108826972M, centered at 10.0°N, 98.4°E). (**B**) A similar wrinkle-ridge ring in volcanic plains in Hesperia Planum, Mars (30°S, 115°E) (portion of Mars Express High-Resolution Stereo Camera nadir image h2660_0001).

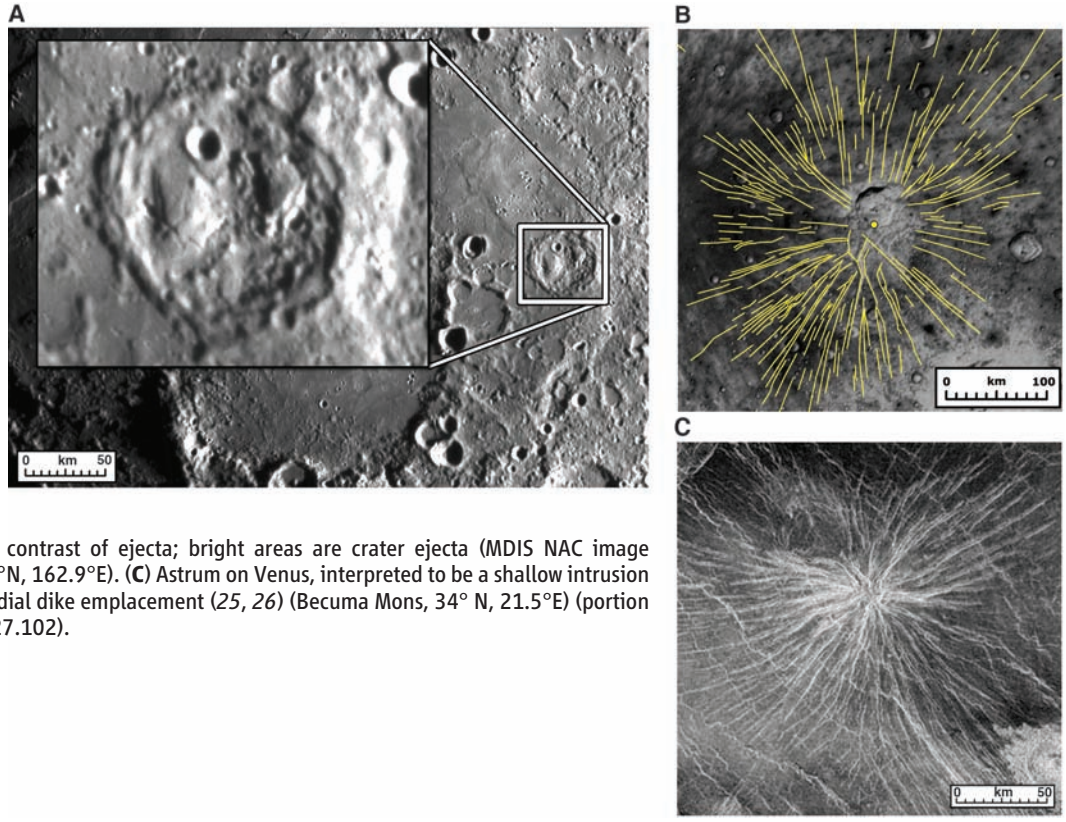

Fig. 4. Floor-fractured crater and radial graben structure, suggestive of intrusive processes on Mercury, as compared with a structure on Venus. (**A**) Floor-fractured, ~35-km-diameter crater (inset); two mounds on the crater floor show networks of fractures. The floor-fractured crater is near extensive tracts of smooth plains to the west and northwest, interpreted to be of extrusive volcanic origin (Fig. 3A) (mosaic of MDIS NAC images EN0108826972M and EN0108826977M, centered at 6.5°N, 100.5°E). Radial graben structure (Pantheon Fossae) on Mercury and astrum on Venus: (**B**) Sketch map of graben radiating from near the center of the Caloris basin, superposed on MESSENGER MDIS image shown as negative to enhance the visual contrast of ejecta; bright areas are crater ejecta (MDIS NAC image EN0108828540M, centered at 29.9°N, 162.9°E). (**C**) Astrum on Venus, interpreted to be a shallow intrusion surrounded by graben formed by radial dike emplacement (*25*, *26*) (Becuma Mons, 34° N, 21.5°E) (portion of Magellan image C1-MIDR.30N027.102).

ized nature of the floor fractures favors intrusion over broader-scale relaxation.

A second candidate for magmatic intrusion is Pantheon Fossae, a radial graben structure in the center of the Caloris basin (*15*). Over 100 graben, typically 2 to 3 km wide and tens to hundreds of kilometers long, radiate away from the center. Several hypotheses are being assessed for the origin of this feature (*15*) (Fig. 4B), but one possible mechanism—which was proposed for morphologically similar features (astra) on Venus (Fig. 4C)—is that rising magma forms a reservoir at a neutral buoyancy zone below the surface, and over-pressurization of the reservoir results in emplacement of radial dikes. Shallow radial dikes imply that the near-surface stress field is extensional; as a result, graben tend to form over the dikes. Under some conditions, dikes will give rise to associated extrusive volcanism, whereas under other conditions, dikes remain largely intrusive (*25*). So far, Pantheon Fossae is the only such radial graben structure observed on Mercury; in contrast, more than 60 astra have been documented on Venus (*26*). The location of the single Mercury example in central Caloris basin might be related to pressure-release melting induced by mantle upwelling localized by basin formation (*27*), in which case additional examples might be sought at the centers of other basins on Mercury.

These data, together with multispectral images and spectra showing evidence for multiple plains units (*16*) of different ages (*28*), substantiate the role of volcanism as an important process in the geological history of Mercury. The volcanic style of Mercury appears to be similar to that of the Moon, with regional volcanic plains filling craters, basins, and intervening areas early in the history of the planet. That style contrasts with the huge volcanic edifices and more extended duration of volcanism on Mars and the plate-boundary and hot spot volcanism on Earth.

References and Notes

1. J. W. Head *et al.*, *Space Sci. Rev.* **131**, 41 (2007).
2. N. J. Trask, J. F. McCauley, *Earth Planet. Sci. Lett.* **14**, 201 (1972).
3. V. R. Oberbeck, *Rev. Geophys. Space Phys.* **13**, 337 (1975).
4. B. C. Murray, R. G. Strom, N. J. Trask, D. E. Gault, *J. Geophys. Res.* **80**, 2508 (1975).
5. R. G. Strom, *Phys. Earth Planet. Inter.* **15**, 156 (1977).
6. D. E. Wilhelms, *Icarus* **28**, 551 (1976).
7. M. C. Malin, *Proc. Lunar Planet. Sci. Conf.* **9**, 3395 (1978).
8. S. M. Milkovich, J. W. Head, L. Wilson, *Meteorit. Planet. Sci.* **37**, 1209 (2002).
9. J. W. Head *et al.*, in *Environmental Effects on Volcanic Eruptions: From Deep Oceans to Deep Space*, T. K. P. Gregg, J. R. Zimbelman, Eds. (Plenum, New York, 2000), pp. 143–178.
10. P. D. Spudis, J. E. Guest, in *Mercury*, F. Vilas, C. R. Chapman, M. S. Matthews, Eds. (Univ. of Arizona Press, Tucson, AZ, 1988), pp. 118–164.
11. D. E. Wilhelms, *U.S. Geol. Surv. Prof. Pap.* **1348**, 1 (1987).
12. M. S. Robinson, P. G. Lucey, *Science* **275**, 197 (1997).
13. R. G. Strom, N. J. Trask, J. E. Guest, *J. Geophys. Res.* **80**, 2478 (1975).
14. S. C. Solomon, R. L. McNutt Jr., R. E. Gold, D. L. Domingue, *Space Sci. Rev.* **131**, 3 (2007).
15. S. L. Murchie *et al.*, *Science* **321**, 73 (2008).
16. M. S. Robinson *et al.*, *Science* **321**, 66 (2008).
17. R. J. Pike, in *Mercury*, F. Vilas, C. R. Chapman, M. S. Matthews, Eds. (Univ. of Arizona Press, Tucson, AZ, 1988), pp. 165–273.
18. J. W. Head, A. Gifford, *Moon Planets* **22**, 235 (1980).
19. B. K. Lucchitta, H. H. Schmitt, *Proc. Lunar Sci. Conf.* **5**, 223 (1974).
20. J. W. Head, *Moon Planets* **26**, 61 (1982).
21. T. R. Watters, *J. Geophys. Res.* **98**, 17049 (1993).
22. J. L. Hall, S. C. Solomon, J. W. Head, *J. Geophys. Res.* **86**, 9537 (1981).
23. P. H. Schultz, *Moon* **15**, 241 (1976).
24. P. H. Schultz, *Phys. Earth Planet. Inter.* **15**, 202 (1977).
25. E. A. Parfitt, J. W. Head, *Earth Moon Planets* **61**, 249 (1993).
26. A. Krassilnikov, J. W. Head, *J. Geophys. Res.* **108**, 5108 (2003).
27. L. T. Elkins-Tanton, B. H. Hager, T. L. Grove, *Earth Planet. Sci. Lett.* **222**, 17 (2004).
28. R. G. Strom *et al.*, *Science* **321**, 79 (2008).
29. S. C. Solomon *et al.*, *Science* **321**, 59 (2008).
30. We thank the MESSENGER mission instrument, planning, and operations teams. R. L. McNutt Jr., D. L. Domingue, and S. E. Hawkins III provided leadership in mission planning and instrument design; N. Laslo, H. Kang, R. Vaughan, A. Harch, R. Shelton, and A. Berman designed the imaging sequences; and B. Denevi, K. Becker, and C. Hash provided data calibration and processing. We thank S. Schneider, J. Dickson, C. Fassett, L. Kerber, D. Hurwitz, G. Morgan, S. Schon, L. Ostrach, and N. Chabot for support. The MESSENGER project is supported by the NASA Discovery Program under contracts NAS5-97271 to the Johns Hopkins University Applied Physics Laboratory and NASW-00002 to the Carnegie Institution of Washington.

17 April 2008; accepted 3 June 2008
10.1126/science.1159256